Applied Physics Letters

# Strongly polarized quantum well infrared photodetector with metallic cavity for narrowband wavelength selective detection

Cite as: Appl. Phys. Lett. **116**, 161107 (2020); https://doi.org/10.1063/5.0002012
Submitted: 21 January 2020 . Accepted: 30 March 2020 . Published Online: 21 April 2020

Xiaofei Nie, Honglou Zhen, Gaoshan Huang, Yizhe Yin, Shilong Li, Pingping Chen, Xiaohao Zhou, Yongfeng Mei, and Wei Lu

Applied Physics Letters ARTICLE scitation.org/journal/apl

# Strongly polarized quantum well infrared photodetector with metallic cavity for narrowband wavelength selective detection

Cite as: Appl. Phys. Lett. **116**, 161107 (2020); doi: 10.1063/5.0002012
Submitted: 21 January 2020 · Accepted: 30 March 2020 ·
Published Online: 21 April 2020



Xiaofei Nie,[1,2] Honglou Zhen,[1,2] Gaoshan Huang,[3] Yizhe Yin,[1,4] Shilong Li,[1,2] Pingping Chen,[1,2] Xiaohao Zhou,[1,2] Yongfeng Mei,[3,a)] and Wei Lu[1,2,b)]

## AFFILIATIONS

[1]Key Laboratory of Infrared Physics, Shanghai Institute of Technical Physics, Chinese Academy of Sciences, Shanghai 200083, People's Republic of China
[2]University of Chinese Academy of Sciences, Beijing 100049, People's Republic of China
[3]Department of Materials Science and State Key Laboratory of ASIC and system, Fudan University, Shanghai 200433, People's Republic of China
[4]Mathematics and Science College, Shanghai Normal University, Shanghai 200234, People's Republic of China

[a)]**Author to whom correspondence should be addressed:** yfm@fudan.edu.cn
[b)]**E-mail:** luwei@mail.sitp.ac.cn

## ABSTRACT

A quantum well-integrated metallic microcavity infrared photodetector is designed and fabricated to achieve highly polarized narrowband wavelength selective detection. Linear grooves are etched on top of the mesa and then the whole device is completely coated with Ti/Au to form an open metallic microcavity, and the resonant mode of the metallic cavity can be detected by the embedded quantum well active layer. The obtained devices show very narrow wavelength selective detection ability as well as strong polarization-dependent characteristics. High performances such as a quality factor of 60 and a polarization extinction ratio of 146 are noticed. Our work provides a promising basis for developing highly integrated infrared cameras with a remarkable performance.



Multispectral and/or polarization imaging are inevitable requirements for the next generation of infrared cameras.[1–9] Compared to monochrome/panchromatic imaging, narrow and multispectral imaging can provide more abundant object information, making it possible to determine the absolute temperature of the object, and reducing the sensitivity of the camera to atmospheric conditions. The combination of several adjacent spectral channels facilitates the detection of buried objects in a complex environment.[5] Artificial objects (such as metal and glass) normally have different polarization characteristics to that of natural objects. Acquiring polarization information therefore has the potential to identify certain objects, and is considered to be an important means to improve the identification efficiency and reduce false alarms.[2–4] Traditional multispectral and polarization technologies are based on the incorporation of a single spectral focal plane array, spectrometers, and/or polarizers, which often require a high-cost mechanical scanning instrument and extra space. These additional instruments also require additional refrigeration to suppress their own infrared radiation, especially for long-wavelength infrared detection, and therefore lead to high cooling power.[1–3]

In order to achieve a multi-functional infrared detector with high performance, tremendous efforts have been dedicated to integrate camera pixels with spectral or polarization detection ability,[10–23] such as the Fabry–Pérot filter,[14,15] plasmonic filter,[16–19] lenslet array,[23] and micropolarizers.[19–22] In most cases, the quality factor [*Q-factor*, which is defined as the ratio of resonant mode wavelength and the full width of half maximum (FWHM) of the mode] and the polarization extinction ratio (PER, which is defined as the ratio of the maximum and minimum response), are used to evaluate the device performance. However, the reported *Q-factor* is less than 16 at the wavelength of 1.5–4 $\mu$m[23] and the PER does not exceed 13 at the wavelength of 3–5 $\mu$m.[20] On the other hand, quantum well infrared photodetectors (QWIPs) with various coupling structures (3D tubular, resonator or

optical polarimetric coupling structures) have shown their superiority on wide angle detection, room temperature operation, narrowband detection, and/or polarization detection.[24–34] Previous studies found that the mesa structures in QWIPs can be directly used as resonators or polarimetric coupling structures (such as sub-wavelength metallic resonators,[25] diffractive optics resonant cavity,[26] quantum grid,[27,28] lamellar gratings,[29–31] and metal-dielectric-metal plasmonic microcavity[32]) to further improve the device performance. Although the PER could be large,[32] the resonance in these structures is produced by the refraction index mismatch and such a weak bound cavity can hardly lead to a very narrow response.[26–32] That is, to achieve a high *Q-factor* and a large *PER* simultaneously is challenging.

In this Letter, we design and fabricate QWIPs with a metallic cavity (MC-QWIP), which not only achieve very narrow wavelength selective detection but also have a very high PER. The FWHM achieved by our prototype device is as narrow as 0.095 $\mu$m at 5.71 $\mu$m, resulting in a *Q-factor* as high as 60 and the PER achieved by our prototype device is as high as 146 at 9.13 $\mu$m. We also experimentally and theoretically study the influence of device geometry on the detection performance of the device. The promoted performance makes the current device promising in providing multispectral and polarization information, which is considered essential for the next generation of infrared photodetectors.

The structure of MC-QWIP is schematically shown in Fig. 1(a), and two multilayered QW materials with bottom contacts of different thicknesses (denoted as M1 and M2, see Fig. S1 in the supplementary material) were used for device fabrication. In the current design of MC, one or two linear grooves are etched on the top of the mesa in order to couple more incident light into the cavity, and the $HfO_2$ film is used to prevent short circuit caused by Ti/Au on the sidewall. Figure 1(b) shows the scanning electron microscopy (SEM) image and the transmission electron microscopy (TEM) image (inset) of the cross section of an MC-QWIP. The images prove that the MC is formed by a Ti/Au coating as expected. In addition, the morphological characterization shows that the $HfO_2$ film has a superior step coverage ensuring reliable insulation between the Ti/Au and the QWIP mesa.

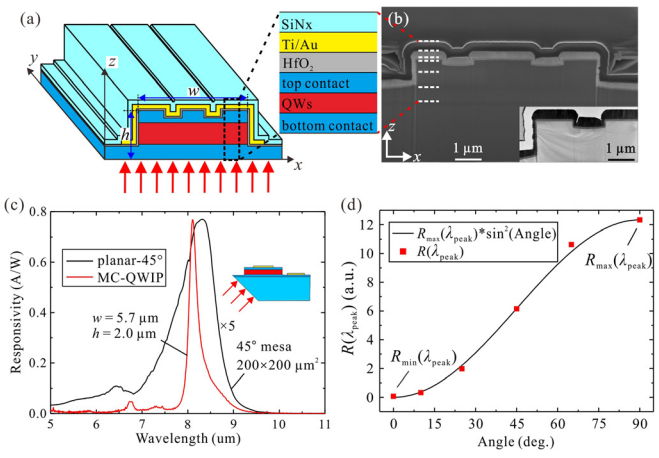


**FIG. 1.** (a) Schematic diagram of an MC-QWIP. The multi-layered structure is illustrated in the inset. (b) SEM image and TEM image (inset) of the cross section of an MC-QWIP. The layers are highlighted by the dashed lines. (c) Responsivity measured at 40 K with 2 V bias. Red and black (5 times magnification) lines are obtained from **the** MC-QWIP and a planar device with a 45° edge facet, respectively. The black line is five times magnification. The inset schematically shows the structure of the planar device. (d) Response $R(\lambda_{peak})$ as a function of the polarization angle.

When infrared light propagating along the *z*-axis illuminates the device from the bottom side, standing waves of certain wavelengths are generated in the MC and give rise to cavity modes. The responsivity of the device made from M1 with width $w = 5.7\ \mu$m and $h = 2.0\ \mu$m was measured [red line in Fig. 1(c)], and the result obtained from a $200 \times 200\ \mu m^2$ planar device made from M1 with a 45° edge facet [inset of Fig. 1(c)] is also demonstrated as a black line (5 times magnification) in Fig. 1(c) for comparison. It is worth noting that the spectrum of the device with a 45° edge facet gives the intrinsic absorption characteristic of the QW material (see Fig. S2 in the supplementary material).[35] The spectrum of the MC-QWIP exhibits an enhanced response peak (about 5 times compared with the response of the 45° device) at 8.12 $\mu$m with an FWHM of 0.22 $\mu$m (*Q-factor* of 36.9) which is much narrower than that of the intrinsic broad response spectrum, indicating a strong resonant mode within the MC. Besides the narrowband characteristic and response enhancement, the MC-QWIP also has strong polarization dependence. The polarization dependent photocurrent spectra of an MC-QWIP made from M2 with $w = 6.4\ \mu$m and $h = 2.2\ \mu$m were obtained by rotating the polarization of the incident light in the *xy*-plane (see Fig. S3 in the supplementary material). Figure 1(d) shows the response at the peak of the spectrum $R(\lambda_{peak})$ as a function of the polarization angle, and the calculated PER is ~146, which is higher than the previous record of 136 in the literature.[32] The polarization response of the MC-QWIP has a sine-squared dependence on the polarization angle, which is the same as the polarization characteristic of a 45° device.[25] Nevertheless, the MC-QWIP has the advantage of easily being fabricated into the focal plane array. Such a highly integrated device with a narrow band characteristic and strong polarization dependence is promising in acquiring high dimensional infrared image data (including spatial, spectral, and polarization information).[6,30,31]

For practical applications, the response of the device should be tunable.[26–31] In our experiment, we indeed notice that the resonant wavelengths of the MC-QWIPs can be tuned by the mesa width *w* (Fig. 2) and the cavity height *h* (see Fig. S4 in the supplementary material). The experimental results in Figs. 2(a), 2(b), and S4 demonstrate that for the obtained devices, the resonant wavelength shifts to a longer wavelength with an increasing mesa size (*w* and *h*).

In the case of resonance, the incident electromagnetic wave should form a standing wave. The distribution of the electric field in the *z* direction $E_z$ and resonance of the MC are carefully studied with the help of the simulation.[36,37] In the simulation, the incident light was set as an *x*-polarized plane electromagnetic wave with the electric field amplitude $E_0$ and illuminated the MC-QWIP from the bottom side. Figures 2(c)–2(f) show the simulated distribution of $E_z/E_0$ for the MC-QWIPs at resonant wavelengths. Figure 2(c) corresponds to the MC-QWIP made from M1 with $w = 5.6\ \mu$m and $h = 2.0\ \mu$m and Figs. 2(d)–2(f) represent three different modes from MC-QWIP made from M1 with $w = 8.4\ \mu$m and $h = 2.0\ \mu$m. The pattern of the standing wave can be clearly observed in all the simulations. Here, the numbers of peaks and valleys of $E_z$ distribution in the horizontal and vertical directions, (*M*, *N*), can be used to identify the cavity mode.[38] Accordingly, the experimental resonant modes in the Fig. 2(a) are

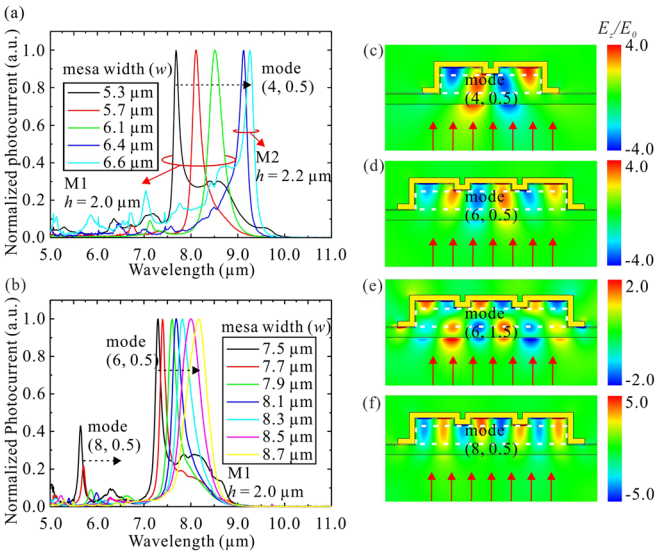


**FIG. 2.** The normalized photocurrent spectra of the fabricated MC-QWIPs with different mesa widths: (a) $w = 5.3$–$6.6\ \mu$m and (b) $w = 7.5$–$8.7\ \mu$m. The devices are illuminated by unpolarized light during measurement. (c)–(f) The simulated $E_z/E_0$ distribution for MC-QWIPs made from M1 at resonant wavelengths. $E_0$ is the electric field amplitude of the *x*-polarized incident light. The width and height are 5.6 and 2.0 $\mu$m, respectively, for (c) and 8.4 and 2.0 $\mu$m, respectively, for (d)–(f). The white boxes in (c)–(f) indicate the QW active layer, and the mode numbers are marked.

identified as mode (4, 0.5) and the modes in Fig. 2(b) are identified as mode (8, 0.5) and (6, 0.5). The resonant wavelength shifts to longer wavelengths with increasing mesa widths for all the modes. In addition, Figs. 2(a) and 2(b) further demonstrate that the FWHMs of the photocurrent spectra of MC-QWIPs are much narrower than that of the QW's intrinsic response (see Fig. S2). For instance, the mode (8, 0.5) of the device with $w = 7.7\ \mu$m [red curve in Fig. 2(b)] at 5.71 $\mu$m has an FWHM of 0.095 $\mu$m, resulting in a high *Q-factor* of ~60. In addition, the spectrum of the device with $w = 7.5\ \mu$m [black curve in Fig. 2(b)] exhibits two notable peaks indicating that two strong resonant modes exist in the metallic cavity. They are identified as mode (8, 0.5) and (6, 0.5), respectively. With the increasing of *w*, mode (8, 0.5) becomes weak and finally disappears. This is because an optimized cavity structure is required for a specific mode to achieve effective coupling. The change of the cavity structure leads to deviation of the resonance condition and thus the weakening of the mode.

We have demonstrated the potential of the MC-QWIP in narrowband wavelength selective detection and polarization detection. With the increase in the mesa width *w* or cavity height *h*, the resonant wavelength shifts to a longer wavelength. In the case of vertical incident light, the resonant wavelength of each mode can be roughly estimated by the following equation:

$$\lambda = \frac{2n_{eff}}{\sqrt{\left(\frac{M}{w}\right)^2 + \left(\frac{N}{h}\right)^2}}, \quad (1)$$

where $n_{eff}$ is the effective refraction index of the medium within the metallic cavity.[38]

The relations between the resonant wavelengths and the cavity sizes predicted by Eq. (1) are shown in Fig. 3. The resonant wavelengths and the *Q-factors* extracted from the measured photocurrent spectra are also displayed. The theoretically predicted resonant wavelengths agree well with the experimental results, and the small deviation is attributed to the inaccuracy of the cavity's effective size as well as the effective refractive index of the cavity material. Specifically, the $HfO_2$ coating on the mesa results in a bigger cavity while the grooves on the top of the mesa would reduce the "volume" of the cavity. Besides, the cavity formed by the Ti/Au film has an opening at the bottom which reduces the "quality" of the resonator. It is worth noting that the effective refraction index of 3.1 was adopted in the calculation of Eq. (1) to fit the experimental results. However, in the concerned wavelength range, the refraction index of the QW material should decrease as the wavelength increases.[39] As can be seen in Fig. 3, this simplification would lead to a deviation of the resonant wavelength to a longer wavelength since a constant effective refraction index is used.

We also investigate the factors that affect the *Q-factors* of the devices. The peaks of intrinsic response spectra of M1 and M2 are at 8.32 and 8.53 $\mu$m, respectively. It seems that the closer the resonant wavelength approaches to the intrinsic absorption peak, the wider the resonant spectrum is (or the smaller the *Q-factor* is). This is probably due to the increased loss from the quantum well absorption.[26–28] In addition, by examining the *Q-factors* of the (6, 0.5) mode at ~8.0 $\mu$m, we find that the *Q-factor* of the mode decreases when the *h* decreases. The influence of the height is also reflected by the fact that the *Q-factors* of devices made from M1 are generally smaller than that from M2. In addition, for the devices with the same design, there may also be a tiny difference in the structure caused by processing like the etching step. All these influence factors lead to quality differences of the MC and give rise to different *Q-factors*. Nevertheless, the co-effect of MC with high quality and QW with low absorption results in a narrow response of MC-QWIP.

From Eq. (1) and the current experimental results, both the cavity width and height affect the cavity resonant mode. When the width of the metal cavity becomes larger (for example, the pixel size is ~30 $\mu$m), the cavity mode will be much more complicated. Similarly, the height of the cavity will also affect the resonant mode. An optimal cavity height is required to reduce the reflection of incident light and

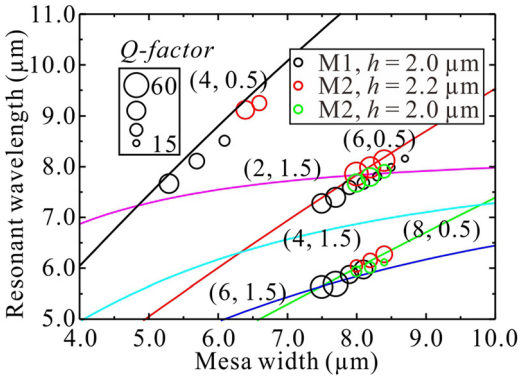


**FIG. 3.** Resonant wavelengths (and *Q-factors*) of different modes vs the mesa width *w*. The circles are extracted from the measurements and the solid lines are calculated according to Eq. (1). Here, $n_{eff} = 3.1$ are employed in the calculation.

ensure total internal reflection at the bottom interface, thereby ensuring multiple cycles of light in the cavity. For a detection wavelength of $\sim 8\,\mu$m, an optimal height of the cavity is $\sim 2\,\mu$m. Simulation work shows that the grooves on the top surface of the mesa play an important role in exciting the desired cavity mode. Matching the period and number of grooves to the cavity mode will help to select and enhance the resonance of a mode [for example, mode (M, 0.5)]. A qualitative explanation is that when the incident light enters the cavity, due to the reflection of the metal wall and the bottom interface, the incident light will be diffracted by the grooves and then circulated in the cavity before being completely absorbed or dissipated. If there is a match between the groove and cavity modes, the cavity mode is repeatedly enhanced during the cycle of light. Although large pixels are needed today to achieve a high optical response, a large format and small pixel focal plane arrays are also future trends. Exploring a clearer mechanism and correspondingly developing a better MC-QWIP will be carried out in our subsequent work.

In summary, MC-QWIP is fabricated by coating the Ti/Au film on the QWIP mesa resulting in an integration of MC and QW sensor pixel. The resonance produced by the MC ensures a very narrow and tunable response spectrum of the detector. The *Q-factors* of most resonant modes are 30–50, and the highest is as high as 60 at 5.71 $\mu$m. The MC-QWIP is strongly polarization-dependent, and the PER achieved is as high as 146 at 9.13 $\mu$m. Since the resonance can be conveniently tuned and manipulated by the geometry of the mesa, many novel infrared imaging cameras or spectrometers could be realized by using such a versatile detector.

See the supplementary material for the details of the device simulation, fabrication, and measurement, as well as the measured photocurrent spectra.

## AUTHOR'S CONTRIBUTIONS

X.N. and H.Z. contributed equally to this work.

We acknowledge the financial support from the National Natural Science Foundation of China (Nos. 61521005 and 61991444) and the Science and Technology Commission of Shanghai Municipality (Nos. 19ZR465600, 18JC1420401, and 18ZR1405100).

## REFERENCES

[1]C. D. Tran, "Principles, instrumentation, and applications of infrared multispectral imaging, an overview," Anal. Lett. **38**, 735 (2005).
[2]J. S. Tyo, D. L. Goldstein, D. B. Chenault, and J. A. Shaw, "Review of passive imaging polarimetry for remote sensing applications," Appl. Opt. **45**, 5453 (2006).
[3]J. R. Schott, *Fundamentals of Polarimetric Remote Sensing* (SPIE Press, Washington, 2009).
[4]J. Duan, Q. Fu, C. Mo, Y. Zhu, and D. Liu, "Review of polarization imaging for international military application," Proc. SPIE **8908**, 890813 (2013).
[5]A. Rogalski, J. Antoszewski, and L. Faraone, "Third-generation infrared photodetector arrays," J. Appl. Phys. **105**, 091101 (2009).
[6]N. A. Hagen, L. S. Gao, T. S. Tkaczyk, and R. T. Kester, "Snapshot advantage: A review of the light collection improvement for parallel high-dimensional measurement systems," Opt. Eng. **51**, 111702 (2012).
[7]N. Hagen and M. W. Kudenov, "Review of snapshot spectral imaging technologies," Opt. Eng. **52**, 090901 (2013).
[8]R. Bhargava, "Infrared spectroscopic imaging: The next generation," Appl. Spectrosc. **66**, 1091 (2012).
[9]R. Ivanov, S. Smuk, S. Hellström, D. Evans, L. Höglund, and E. Costard, "LWIR QWIPs at IRnova for next generation polarimetric imaging," Infrared Phys. Technol. **95**, 177 (2018).
[10]J. W. Stewart, G. M. Akselrod, D. R. Smith, and M. H. Mikkelsen, "Toward multispectral imaging with colloidal metasurface pixels," Adv. Mater. **29**, 1602971 (2017).
[11]Y. Hui, J. S. Gomez-Diaz, Z. Qian, A. Alù, and M. Rinaldi, "Plasmonic piezoelectric nanomechanical resonator for spectrally selective infrared sensing," Nat. Commun. **7**, 11249 (2016).
[12]S. Ogawa and M. Kimata, "Wavelength- or polarization-selective thermal infrared detectors for multi-color or polarimetric imaging using plasmonics and metamaterials," Materials **10**, 493 (2017).
[13]T. D. Dao, S. Ishii, A. T. Doan, Y. Wada, A. Ohi, T. Nabatame, and T. Nagao, "An on-chip quad-wavelength pyroelectric sensor for spectroscopic infrared sensing," Adv. Sci. **6**, 1900579 (2019).
[14]L. Frey, L. Masarotto, M. Armand, M.-L. Charles, and O. Lartigue, "Multispectral interference filter arrays with compensation of angular dependence or extended spectral range," Opt. Express **23**, 11799 (2015).
[15]R. F. Wolffenbuttel, "State-of-the-art in integrated optical microspectrometers," IEEE Trans. Instrum. Meas. **53**, 197 (2004).
[16]C. Genet and T. W. Ebbesen, "Light in tiny holes," Nature **445**, 39 (2007).
[17]A. Safaei, S. Modak, J. Lee, S. Chandra, D. Franklin, A. Vázquez-Guardado, and D. Chanda, "Multi-spectral frequency selective mid-infrared microbolometers," Opt. Express **26**, 32931 (2018).
[18]J. Xu, A. Wang, and Y. Dan, "Plasmonic micropipe spectral filters in mid-infrared," Opt. Lett. **44**, 4479 (2019).
[19]J. Rosenberg, R. V. Shenoi, T. E. Vandervelde, S. Krishna, and O. Painter, "A multispectral and polarization-selective surface-plasmon resonant midinfrared detector," Appl. Phys. Lett. **95**, 161101 (2009).
[20]G. P. Nordin, J. T. Meier, P. C. Deguzman, and M. W. Jones, "Micropolarizer array for infrared imaging polarimetry," J. Opt. Soc. Am. A **16**, 1168 (1999).
[21]W. Chu, W. Chao, C. Xiahui, Y. Yu, B. Ali, and B. Jing, "Chip-integrated plasmonic flat optics for mid-infrared full-Stokes polarization detection," Photonics Res. **7**, 1051 (2019).
[22]S. Ogawa, Y. Takagawa, and M. Kimata, "Broadband polarization-selective uncooled infrared sensors using tapered plasmonic micrograting absorbers," Sens. Actuators, A **269**, 563 (2018).
[23]M. Hinnrichs and J. Jensen, "Simultaneous multispectral imaging using lenslet arrays," Proc. SPIE **8616**, 861615 (2013).
[24]B. F. Levine, "Quantum-well infrared photodetectors," J. Appl. Phys. **74**, R1 (1993).
[25]D. Palaferri, Y. Todorov, A. Bigioli, A. Mottaghizadeh, D. Gacemi, A. Calabrese, A. Vasanelli, L. Li, A. G. Davies, E. H. Linfield, F. Kapsalidis, M. Beck, J. Faist, and C. Sirtori, "Room-temperature nine-$\mu$m-wavelength photodetectors and GHz-frequency heterodyne receivers," Nature **556**, 85 (2018).
[26]P. Mitra, F. C. Case, J. H. McCurdy, S. A. Zaidel, and L. T. Claiborne, "Multispectral long-wavelength quantum-well infrared photodetectors," Appl. Phys. Lett. **82**, 3185 (2003).
[27]K. K. Choi, C. H. Lin, K. M. Leung, T. Tamir, J. Mao, D. C. Tsui, and M. Jhabvala, "Broadband and narrow band light coupling for QWIPs," Infrared Phys. Technol. **44**, 309 (2003).
[28]K. K. Choi, G. Dang, J. W. Little, K. M. Leung, and T. Tamir, "Quantum grid infrared spectrometer," Appl. Phys. Lett. **84**, 4439 (2004).
[29]T. Antoni, A. Nedelcu, X. Marcadet, H. Facoetti, and V. Berger, "High contrast polarization sensitive quantum well infrared photodetectors," Appl. Phys. Lett. **90**, 201107 (2007).
[30]N. Alexandru, G. Vincent, B. Arnaud, B. d l I. Nadia, and H. Odile, "Multispectral and polarimetric imaging in the LWIR: Intersubband detectors as a versatile solution," Infrared Phys. Technol. **59**, 125 (2013).
[31]S. Smuk, R. Ivanov, D. Evans, S. Sehlin, W. Diel, S. Hellström, L. Höglund, A. Smuk, and E. Costard, "QWIPs are keeping their promises," Proc. SPIE **11002**, 110021Y (2019).
[32]Y. W. Zhou, Z. F. Li, J. Zhou, N. Li, X. H. Zhou, P. P. Chen, Y. L. Zheng, X. S. Chen, and W. Lu, "High extinction ratio super pixel for long wavelength infrared polarization imaging detection based on plasmonic microcavity quantum well infrared photodetectors," Sci. Rep. **8**, 15070 (2018).

[33]H. Wang, H. Zhen, S. Li, Y. Jing, G. Huang, Y. Mei, and W. Lu, "Self-rolling and light-trapping in flexible quantum well-embedded nanomembranes for wide-angle infrared photodetectors," Sci. Adv. **2**, e1600027 (2016).
[34]F. Zhang, X. Nie, G. Huang, H. Zhen, F. Ding, Z. Di, and Y. Mei, "Strain-modulated photoelectric properties of self-rolled GaAs/$Al_{0.26}Ga_{0.74}As$ quantum well nanomembrane," Appl. Phys. Express **12**, 065003 (2019).
[35]K. K. Choi, M. D. Jhabvala, J. Sun, C. A. Jhabvala, A. Waczynski, and K. Olver, "Resonator-quantum well infrared photodetectors," Appl. Phys. Lett. **103**, 201113 (2013).
[36]K. K. Choi, J. Sun, E. A. DeCuir, K. A. Olver, and P. Wijewarnasuriya, "Electromagnetic modeling and resonant detectors and arrays," Infrared Phys. Technol. **70**, 153 (2015).
[37]K. K. Choi, "Electromagnetic modeling of edge coupled quantum well infrared photodetectors," J. Appl. Phys. **111**, 124507 (2012).
[38]B. S. Guru and H. R. Hiziroglu, *Electromagnetic Field Theory Fundamentals*, 2nd ed. (Cambridge University Press, Cambridge, 2009).
[39]S. Adachi, "Optical dispersion relations for GaP, GaAs, GaSb, InP, InAs, InSb, $Al_xGa_{1-x}As$, and $In_{1-x}Ga_xAs_yP_{1-y}$," J. Appl. Phys. **66**, 6030 (1989).